Inorganic Chemistry

Article

pubs.acs.org/IC

Variations of Structures and Gas Sorption Properties of Three Coordination Polymers Induced by Fluorine Atom Positions in Azamacrocyclic Ligands

Long Jiang, Xian-Rui Meng, Hua Xiang, Ping Ju, Di-Chang Zhong,* and Tong-Bu Lu*

MOE Key Laboratory of Bioinorganic and Synthetic Chemistry, State Key Laboratory of Optoelectronic Materials and Technologies, and School of Chemistry and Chemical Engineering, Sun Yat-Sen University, Guangzhou 510275, China

Supporting Information

ABSTRACT: Three coordination polymers of $[(NiL^1)_3(TCBA)_2]$ (**1**), $[(NiL^2)_3(TCBA)_2]$ (**2**), and $[(NiL^3)_3(TCBA)_2]$ (**3**) have been constructed using azamacrocyclic Ni(II) complexes $[NiL^1](ClO_4)_2/[NiL^2](ClO_4)_2/[NiL^3](ClO_4)_2$ and $TCBA^{3-}$ as building blocks (L^1 = 3,10-bis(2-fluorobenzyl)-1,3,5,8,10,12-hexaazacyclotetradecane; L^2 = 3,10-bis(3-fluorobenzyl)-1,3,5,8,10,12-hexaazacyclotetradecane; L^3 = 3,10-bis(4-fluorobenzyl)-1,3,5,8,10,12- hexaazacyclotetradecane; $TCBA^{3-}$ = tri(4-carboxy-benzyl)amine). The results of X-ray diffraction analyses reveal that **1** shows a 2D Borromean structure, while **2** and **3** form 2D layer structures, and the 2D layers are further connected by the interlayer F···F interactions in **2** and C−H···F interactions in **3** to generate two 3D porous structures with 1D fluorine atoms interspersed channels. Gas sorption measurements illustrate that the desolvated **2** and **3** can adsorb N_2, H_2, and CO_2 molecules. The different structures and gas sorption properties of **1** and **2**/**3** are mainly induced by the different positions of F atoms in azamacrocycle ligands.

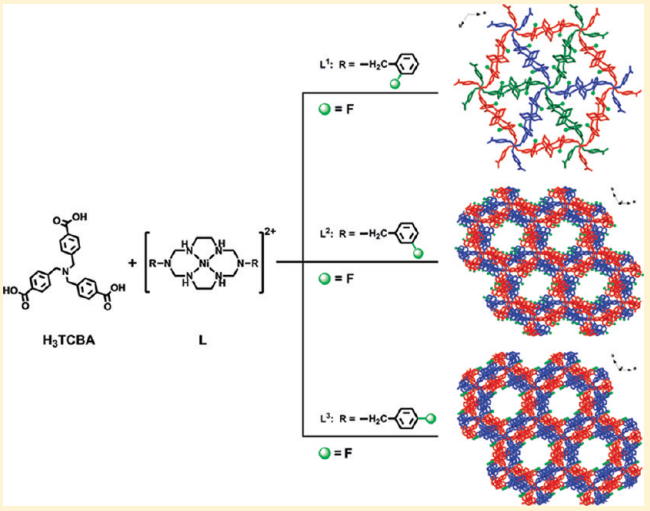

INTRODUCTION

The constructions of porous coordination polymers (PCPs) continue to attract extensive interest because of their variety of architectures and intriguing topologies, as well as potential applications.[1] During the past several years, considerable efforts have been devoted to the design and synthesis of PCPs with unique structures and functions.[2] However, controlled syntheses of such PCPs are still great challenge. A comparatively effective strategy to tune the structures and functions of PCPs is the modification of organic ligands with different substituents.[3] Although the substituents in organic ligands may not participate in the formation of coordination bonds in the processes of self-assembly of PCPs, they can affect the stacking of 3D supramolecular structures via inter/intramolecular hydrogen/halogen bonding interactions, halogen/halogen contacts, and hydrophilic/hydrophobic interactions.

Recently, the organic ligands with fluorine substituent are used as building blocks for the constructions of PCPs.[4] The main reason is that the fluorine substituent is readily to join the formations of hydrogen bonds or halogen bonds, which can not only stabilize the frameworks of PCPs, but also tune the structures of PCPs. In addition, macrocyclic nickel(II) complexes can provide fixed numbers of vacant coordination sites at the fixed positions and enable the extending direction of the network to be controllable.[5] Very recently, we used macrocyclic nickel(II) complexes and 1,3,5-benzenetricarboxylate as building blocks to construct two 2D nickel(II) PCPs, and we found that the structures and gas sorption properties of two 2D nickel PCPs can be tuned via altering the positions of fluorine atoms in azamacrocyclic ligands.[6] To obtain PCPs with larger pores, and to further understand how the structures and properties of PCPs can be tuned by the fluorine substituent in azamacrocyclic ligands, a new tripodal carboxylic ligand tri(4-carboxy-benzyl)amine (H_3TCBA, Scheme 1) was synthesized, and used to construct PCPs with three azamacrocyclic nickel(II) complexes containing fluorine substituent (Scheme 1). Herein, we reported the synthesis, structures, and gas sorption properties of three coordination polymers of $[(NiL^1)_3(TCBA)_2]$ (**1**), $[(NiL^2)_3(TCBA)_2]$ (**2**), and $[(NiL^3)_3(TCBA)_2]$ (**3**) (L^1 = 3,10-bis(2-fluorobenzyl)-1,3,5,8,10,12- hexaazacyclotetradecane; L^2 = 3,10-bis(3-fluorobenzyl)-1,3,5,8,10,12-hexaazacyclo tetradecane; L^3 = 3,10-bis(4-fluorobenzyl)-1,3,5,8,10,12-hexaazacyclotetradecane, Scheme 1).

Received: October 6, 2011
Published: January 9, 2012

Scheme 1. Sructures of H_3TCBA (Left) and $[NiL^1]^{2+}$/$[NiL^2]^{2+}$/$[NiL^3]^{2+}$ (Right)

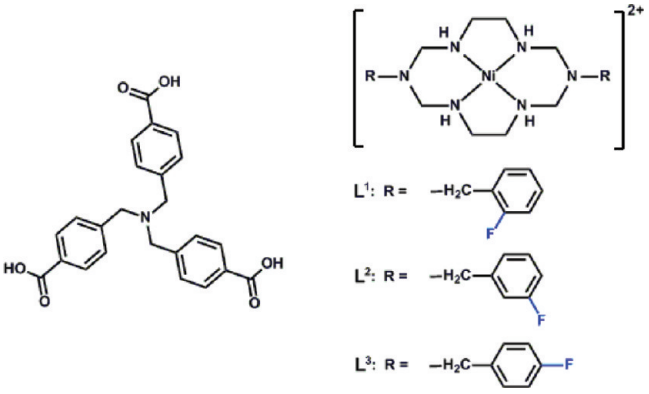

EXPERIMENTAL SECTION

$[NiL^1](ClO_4)_2$, $[NiL^2](ClO_4)_2$, and $[NiL^3](ClO_4)_2$ were prepared according to the previously reported methods.[6] All of the other chemicals were commercially available and used without further purification. Elemental analyses were determined using Elementar Vario EL elemental analyzer. The IR spectra were recorded in the 4000−400 cm^{-1} region using KBr pellets and a Bruker EQUINOX 55 spectrometer. TG analysis were performed on a Netzsch TG 209 instrument under nitrogen atmosphere with a heating rate of 10 °C/min. Variable-temperature powder X-ray diffraction measurements were performed on a Bruker D8 ADVANCE X-ray diffractometer.

Caution! *Perchlorate salts of metal complexes with organic ligands are potentially explosive. They should be handled with care, and prepared only in small quantities.*

H_3TCBA. A mixture of 4-(bromomethyl)benzoic acid (2.66 g, 12 mmol), 4-(aminomethyl)benzoic acid (0.77 g, 5 mmol), and potassium carbonate (2.30 g, 17 mmol) in 1,4-dioxane (30 mL) was refluxed at 110 °C for two days. After cooling to room temperature, the solvent was evaporated under reduced pressure. The solid residue was extracted with methanol to separate the product and potassium carbonate. After removing the methanol under reduced pressure, the product was recrystallized in methanol and acetone (v/v = 1/1) to give the white powder of H_3TCBA (1.72 g, 82% yield based on 4-(aminomethyl)benzoic acid). ESI-MS (m/z): 418.3 (M − 1). Anal. Calcd for $C_{24}H_{21}O_6N$: C 68.73, H 5.05, N 3.34. Found: C 68.56, H 5.61, N 3.32%. IR (KBr pellet, cm^{-1}): 3395 (m), 2922 (w), 1595 (vs), 1550 (vs), 1391 (vs), 1275(w), 1098 (m), 775 (s). ^{1}H NMR (300 MHz, D_2O) δ 7.74 (m, 6H), 7.32 (m, 6H), 3.53 (m, 6H).

$[(NiL^1)_3(TCBA)_2]$ (1). An aqueous solution (2 mL) of H_3TCBA (0.017 g, 0.04 mmol) and NaOH (0.005 g, 0.12 mmol) was layered with a DMF solution (3 mL) of $[NiL^1](ClO_4)_2$ (0.040 g, 0.06 mmol) at room temperature. After about six days, pink crystals suitable for X-ray analysis formed. Yield: 0.015 g, 30% based on $[NiL^1](ClO_4)_2$. Anal. Calcd for $C_{120}H_{152}N_{22}O_{17}F_6Ni_3$ (**1**·2DMF·3H_2O): C 58.48, H 6.22, N 12.50. Found: C 58.00, H 6.28, N 12.94%. IR (KBr pellet, cm^{-1}): 3411 (w), 3286 (m), 3141 (s), 3047 (w), 2931 (s), 2863 (s), 1682 (vs), 1594 (vs), 1554 (vs), 1493 (m), 1454 (m), 1379 (vs), 1270 (w), 1235 (m), 1146 (w), 1079 (m), 1032 (s), 764 (vs).

$[(NiL^2)_3(TCBA)_2]$ (2). Pink crystals of **2** were obtained by a procedure similar to that of **1** except using $[NiL^2](ClO_4)_2$ instead of $[NiL^1](ClO_4)_2$. Yield: 0.017 g, 29% based on $[NiL^2](ClO_4)_2$. Anal. Calcd for $C_{132}H_{210}N_{26}O_{36}F_6Ni_3$ (**2**·6DMF·18H_2O): C 52.37, H 6.99, N 12.03. Found: C 52.68, H 6.82, N 12.05%. IR (KBr pellet, cm^{-1}): 3413 (w), 3287 (w), 3158 (w), 2928 (m), 2870 (m), 1667 (m), 1594 (s), 1553 (vs), 1487 (w), 1449 (w), 1380 (vs), 1291 (w), 1256 (m), 1183 (w), 1171 (w), 1137 (w), 1071 (w), 1023 (m), 1001 (w), 939 (w), 877 (w), 847 (w), 777 (m), 711 (w), 691 (w), 663 (w), 594 (w), 522 (w), 428 (w).

$[(NiL^3)_3(TCBA)_2]$ (3). Pink crystals of **3** were obtained by a procedure similar to that of **1** except using $[NiL^3](ClO_4)_2$ instead of $[NiL^1](ClO_4)_2$. Yield: 0.009 g, 15% based on $[NiL^3](ClO_4)_2$. Anal. Calcd for $C_{138}H_{206}N_{28}O_{29}F_6Ni_3$ (**3**·8DMF·9H_2O): C 55.04, H 6.90, N 13.02. Found: C 55.36, H 6.91, N, 12.90%. IR (KBr pellet, cm^{-1}): 3158 (w), 2926 (m), 2871 (m), 2867 (m), 1669 (w), 1607 (m), 1599 (vs), 1555 (vs), 1509 (vs), 1464 (w), 1377 (vs), 1270 (w), 1222 (s), 1156 (w), 1074 (m), 1021 (m), 825 (m), 773 (m) cm.

X-ray Structure Determination. Single-crystal X-ray diffraction data for **1**, **2**, and **3** were collected at 293, 123, and 110 K, respectively, on an Oxford Gemini S Ultra diffractometer with the enhance X-ray source of Cu radiation (λ = 1.541 78 Å). All empirical absorption corrections were applied using spherical harmonics implemented in SCALE3 ABSPACK scaling algorithm.[7] The structures were solved by heavy atom methods, which yielded the positions of all nonhydrogen atoms. These were refined first isotropically and then anisotropically. All the hydrogen atoms of the ligands were placed in calculated positions with fixed isotropic thermal parameters and included in structure factor calculations in the final stage of full-matrix least-squares refinement. The positional disorder of fluorobenzyl group in **2** was treated with FVAR with occupancies of 0.691(8) and 0.309(8). The disordered electron density of the heavily disordered DMF and water molecules in **1** was treated as a diffuse contribution using the program SQUEEZE.[8] The hydrogen atoms of disordered lattice water molecules in **2** and **3** were not added. The positional disorder of DMF molecule in **3** was treated with FVAR with occupancies of 0.578(8) and 0.422(8). All of the disordered parts were restrained using DFIX, DELU, and SIMU instructions to make the displacement parameters more reasonable. All calculations were performed using the SHELXTL system of computer programs.[9] The crystallographic data for **1**−**3** are summarized in Table 1, and the selected bond lengths and angles are listed in Table S1.

Gas Sorption Measurements. N_2 and H_2 sorption measurements were performed using a Micromeritics ASAP 2020 instrument, and the CO_2 sorption measurements were carried out on a BELSORP-max automatic volumetric adsorption apparatus. All the adsorption isotherms were collected in a relative pressure range from 10^{-4} to 1.0 atm. The cryogenic temperatures of 77 K required for N_2 and H_2 sorption measurements were controlled by liquid nitrogen, and the 195 K required for CO_2 sorption measurements was controlled using a dry ice−acetone bath. The desolvated samples of **2** (**2d**) and **3** (**3d**) were obtained by heating the samples at 110 °C for 10 h under a high vacuum (less than 10^{-6} mbar). The degassed sample and sample tube were weighed precisely and transferred to the analyzer.

RESULTS AND DISCUSSION

Cystal Structures. Layering an aqueous solution of H_3TCBA and NaOH with a DMF solution of $[NiL^1](ClO_4)_2$/$[NiL^2](ClO_4)_2$/$[NiL^3](ClO_4)_2$ at room temperature gave **1**/**2**/**3**, respectively. As shown in Figure 1, each Ni(II) ion in **1**/**2**/**3** is coordinated to four N atoms from the macrocyclic ligand L^1/L^2/L^3 and two carboxylate O atoms from two individual $TCBA^{3-}$ anions, showing a slightly distorted N_4O_2 octahedral geometry. The Ni−O distances (2.123(3)−2.129(2) Å) in axial positions are slightly longer than the Ni−N distances (2.053(2)−2.074(2) Å) in the equatorial plane (Table S1). In **1**/**2**/**3**, all the three 4-carboxy-benzyl groups in $TCBA^{3-}$ bend to the same side to display a bowl-shaped conformation. Each bowl-shaped $TCBA^{3-}$ bridges three $[NiL^1]^{2+}$/$[NiL^2]^{2+}$/$[NiL^3]^{2+}$ through a C_3 symmetry, and each $[NiL^1]^{2+}$/$[NiL^2]^{2+}$/$[NiL^3]^{2+}$ connects two bowl-shaped $TCBA^{3-}$, generating a 2D (6,3) undulating sheet with honeycomb-like (Figure 2a) or cloverleaf-shaped cavity (Figures 3a and 4a).

In **1**, the diameter of each honeycomb-like cavity is 20 Å (Figure 2a). Such a large cavity allows the honeycomb-shaped sheet to entangle with another two equivalent sheets, forming a 3-fold interpenetrated 2D layer (Figure 2b,c), in which any two of the sheets are not interlocked, but the third sheet makes them impartible (Figure 2b,c). This is the typical and unique characteristic of Borromean structure.[10] The formation of this

dx.doi.org/10.1021/ic202168r | Inorg. Chem. 2012, 51, 1874−1880

Table 1. Crystallographic Data for 1−3

parameter	1	2·6DMF·6H$_2$O	3·6DMF·6H$_2$O
formula	$C_{114}H_{132}O_{12}N_{20}F_6Ni_3$	$C_{132}H_{186}O_{24}N_{26}F_6Ni_3$	$C_{132}H_{186}O_{24}N_{26}F_6Ni_3$
fw	2264.53	2811.12	2811.12
temp (K)	293(2) K	123(2) K	110(2) K
cryst syst	rhombohedral	trigonal	trigonal
space group	$R\bar{3}$	$P\bar{3}c1$	$P\bar{3}c1$
crystal size (mm^3)	0.37 × 0.35 × 0.29	0.35 × 0.28 × 0.20	0.42 × 0.31 × 0.20
a (Å)	16.687(2)	25.2196(2)	25.2592(4)
b (Å)	16.687(2)	25.2196(2)	25.2592(4)
c (Å)	38.706(6)	13.2361(1)	13.1462(3)
α (deg)	90	90	90
β (deg)	90	90	90
γ (deg)	120	120	120
V (Å^3)	9334(2)	7290.66(10)	7263.9(2)
Z/D_c (g cm^{-3})/μ (mm^{-1})	3/1.209/1.116	2/1.286/1.126	2/1.291/1.130
max/min transmission	0.7380/0.6830	0.8061/0.6939	0.8055/0.6482
reflns collected	7538	39398	9353
unique reflns (R_{int})	3286 (0.0379)	3871 (0.0276)	3782 (0.0224)
GOF	0.934	1.090	1.097
R1,[a] wR2[b] (I > 2σ (I))	0.0680, 0.2042	0.0662, 0.2091	0.0441, 0.1466
R1,[a] wR2[b] (all data)	0.0924, 0.2180	0.0690, 0.2140	0.0548, 0.1506

[a] $R_1 = \sum||F_o| - |F_c||/\sum|F_o|$. [b] $wR2 = [\sum[w(F_o^2 - F_c^2)^2]/\Sigma w(F_o^2)^2]^{1/2}$, where $w = 1/[\sigma^2(F_o)^2 + (aP)^2 + bP]$ and $P = (F_o^2 + 2F_c^2)/3$.

Borromean links can be mainly attributed to the large cavities and the undulating nature of the (6,3) sheets.[11] In addition, the C−H···O hydrogen bonding interactions between C4 atom of L^1 in one sheet and O2 atom of $TCBA^{3-}$ in adjacent sheet (C4···O2# = 3.246(8) Å, Figure 2d) may also contribute to the formation of the Borromean structure. Along the c axis, the Borromean layers are parallel stacked together to form a 3D supramolecular structure of **1**. To date, a handful of Borromean structures based on (6,3) network have been reported,[12] while the one constructed by macrocyclic complexes is rare, and only one such structure has been reported so far.[13]

In contrast to **1**, the diameter of each cloverleaf-shaped cavity (11.9 Å) in **2** is much smaller. This results from the fact that two 3-fluorobenzyl groups of L^2 bend to the same cavity (Figure 3a), and decreases the sizes of the cavities. The smaller cavities in **2** cannot allow the sheets to entangle each other. Obviously, the orientation of two fluorobenzyl groups observed in **2** is different from that in **1**, in which the two fluorobenzyl groups in **1** point to two different cavities.

In **2**, there are strong F···F interactions between layers (Figure 3b), and the F···F distance of 2.667(3) Å is close to the literature value of 2.66 Å.[14] It is worth noting that the F···F interactions are not present in the adjacent layers, but exist in every other layer (A···A or B···B, Figure 3b). Through the interlayer F···F interactions, the cloverleaf-shaped (6,3) sheets stack together with an ABAB stacking mode along the c axis to form a 3D porous structure with 1D channels (Figure 3c). The channels, with a diameter of 11.9 Å, are filled with DMF and water molecules. About 30.4% solvent-accessible volume is estimated by using the PLATON program.[15] All the F atoms in L^2 point to the pores, resulting in a F-interspersed pore surface (Figure 3c).

Similar to **2**, the (6,3) undulating sheets in **3** are also cloverleaf-shaped, with two 4-fluorobenzyl groups of L^3 bending to the same cavity (Figure 4a). With an ABAB stacking mode, the cloverleaf-shaped sheets stack together along the c axis to generate a 3D porous structure with 1D channels (Figure 4c). The channels, with a diameter of 11.1 Å, are filled with DMF and water molecules. About 29.7% solvent-accessible volume is estimated by using PLATON program.[15] All the F atoms in L^3 also point to the pores to result in a F-interspersed pore surface (Figure 4c). It should be noted that the interlayer interactions in **3** rely on the C−H···F hydrogen bonds between F atoms in one sheet and H atoms of L^3 in the adjacent sheet (C3···F1#2 = 3.224(8) Å, Figure 4b), instead of C−H···O hydrogen bonds and F···F interactions in **1** and **2**, respectively.

It is interesting to note that, under the same reaction conditions, the different positions of F atoms in azamacrocyclic ligands lead to the formations of different structure of **1** from those of **2** and **3**. The F atoms at 2-fluorobenzyl groups of L^1 do not participate in the formation of hydrogen or halogen bonds, and fluorobenzyl groups locate in the wall of the cavity, resulting in a 2D undulating sheet with large cavities, and the 2D sheets are 3-fold interpenetrated to generate a Borromean structure of **1**. In **2**/**3**, the F atoms at 3/4-fluorobenzyl groups of L^2/L^3 participate in the formations of F···F or C−H···F bonds, leading to the fluorobenzyl groups of L^2/L^3 to bend to the same cavity to result in a 3D porous structure. The different structures between **1** and **2**/**3** may result from the different conformational flexibility of fluorobenzyl groups induced by the different positions of the F atoms. These results indicate that the different positions of the F atoms in the azamacrocyclic ligands can tune the structures of coordination polymers.

XRD and Thermal Analyses. X-ray powder diffraction (XRD) measurements were used to check the phase purity of **1**−**3**. As shown in Figure 5, all the peaks displayed in the measured XRD patterns closely match those in the simulated patterns generated from single-crystal diffraction data, indicating the single phases of **1**−**3** were formed. The variable temperature XPRD measurements indicate that the frameworks of **1**, **2**, and **3** can be stable up to 200, 220, and 200 °C, respectively.

Thermogravimetric measurements for **1**−**3** were carried out from room temperature to 600 °C. As shown in Figure 6, the TG curve of **1** shows a weight loss of 8.2% from room

dx.doi.org/10.1021/ic202168r | Inorg. Chem. 2012, 51, 1874−1880

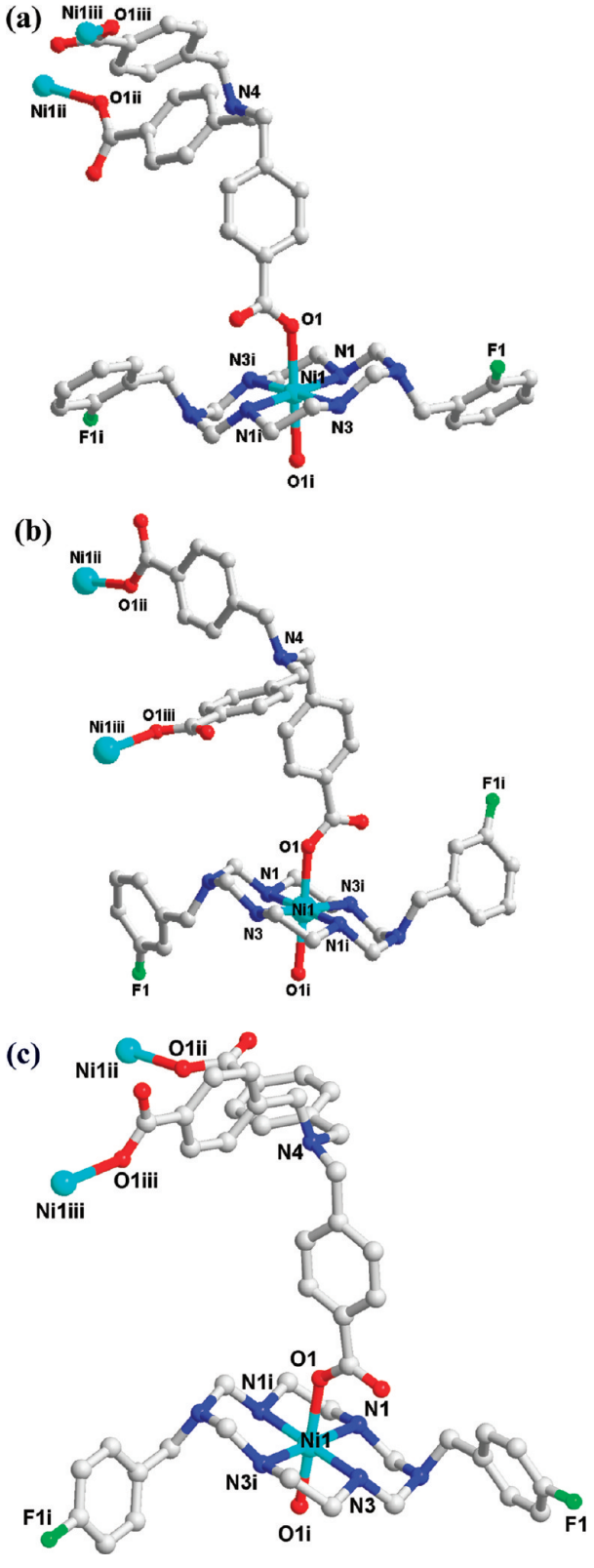

Figure 1. Coordination environments of Ni(II) and the coordination modes of bowl-shaped $TCBA^{3-}$ in (a) **1**, (b) **2**, and (c) **3**, respectively. (Symmetry codes: (i) $^{5}/_{3} - x$, $^{1}/_{3} - y$, $^{1}/_{3} - z$, (ii) $1 - x + y$, $-x$, z, (iii) $-y$, $-1 + x - y$, z for **1**; (i) $2 - x$, $1 - x + y$, $^{1}/_{2} - z$, (ii) $1 - x + y$, $1 - x$, z, (iii) $1 - y$, $x - y$, z for **2**; (i) y, x, $^{1}/_{2} - z$, (ii) $1 - x + y$, $1 - x$, z, (iii) $1 - y$, $x - y$, z for **3**.)

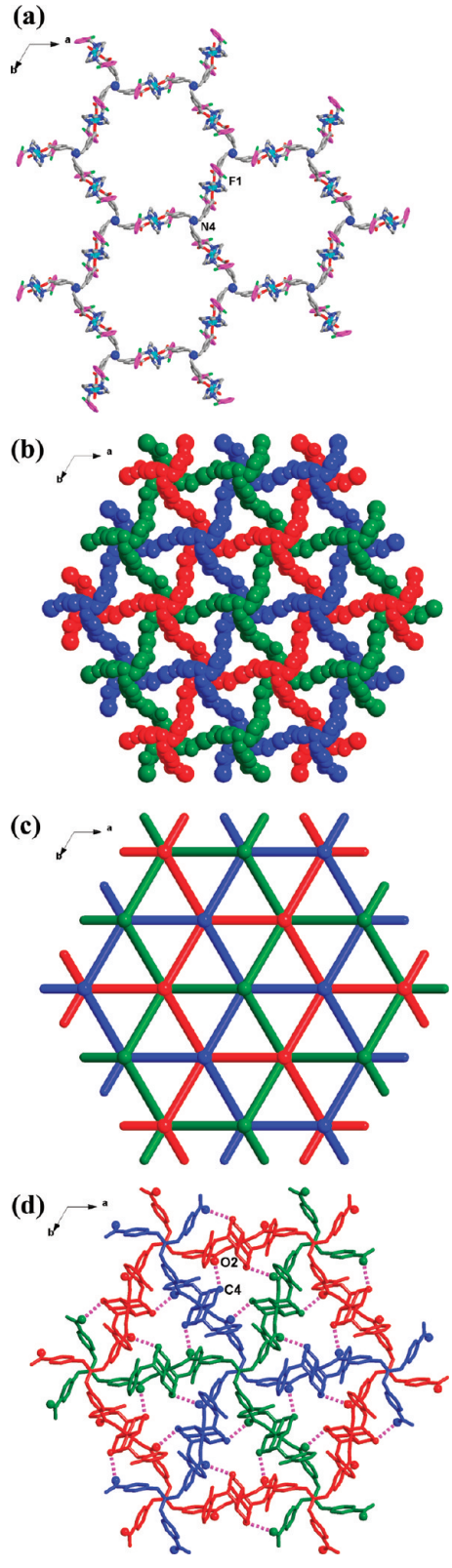

Figure 2. (a) 2D (6,3) sheet of **1**, showing the large honeycomb-like cavities and the tropism of 2-fluorobenzyl groups (in pink). (b) The Borromean links of three separate sheets (the ligands L^1 are omitted for clarity). (c) The topological structure of the Borromean links. (d) The C–H···O hydrogen bonding interactions between the entangled sheets.

temperature to 230 °C, corresponding to the removal of two DMF and three water molecules (calcd 8.1%). Upon further heating, the desolvated framework decomposed through another two steps of weight losses. Compound **2** lost its

dx.doi.org/10.1021/ic202168r | *Inorg. Chem.* 2012, 51, 1874–1880

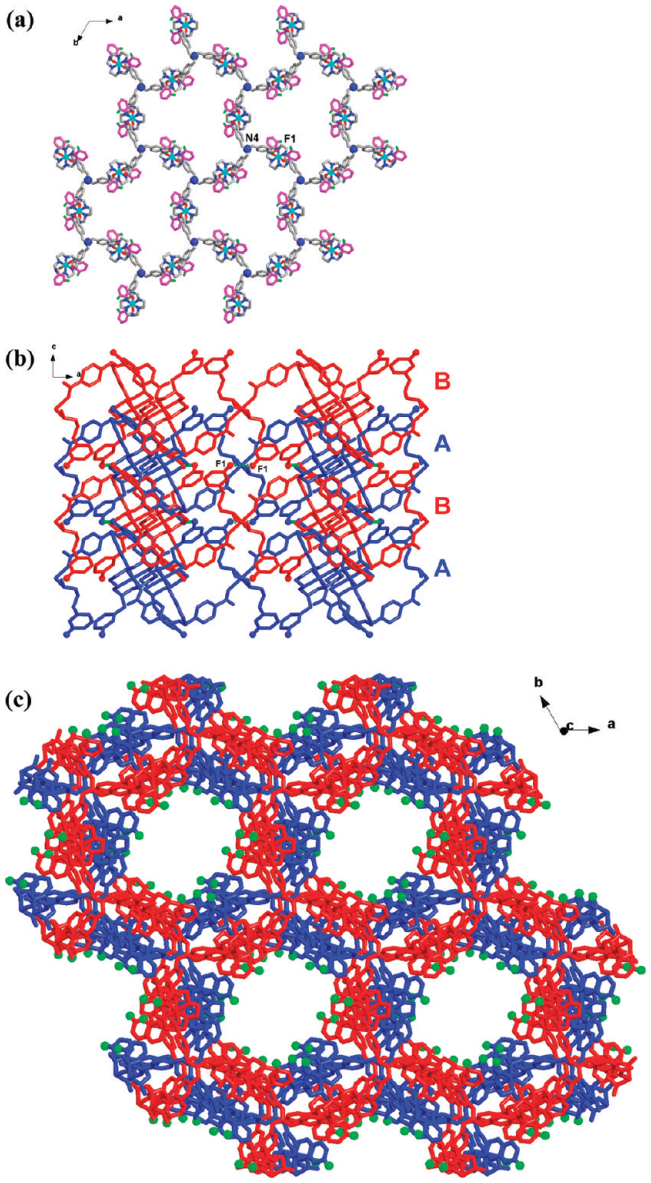

Figure 3. (a) (6,3) sheet of **2**, showing cloverleaf-shaped cavities and the tropism of 3-fluorobenzyl groups (in pink). (b) The ABAB stacking mode in **2**, showing the F···F interactions between every other layers (A···A or B···B). (c) The 3D porous structure of **2** with 1D fluorine atoms (green) interspersed channels (the solvents are omitted for clarity).

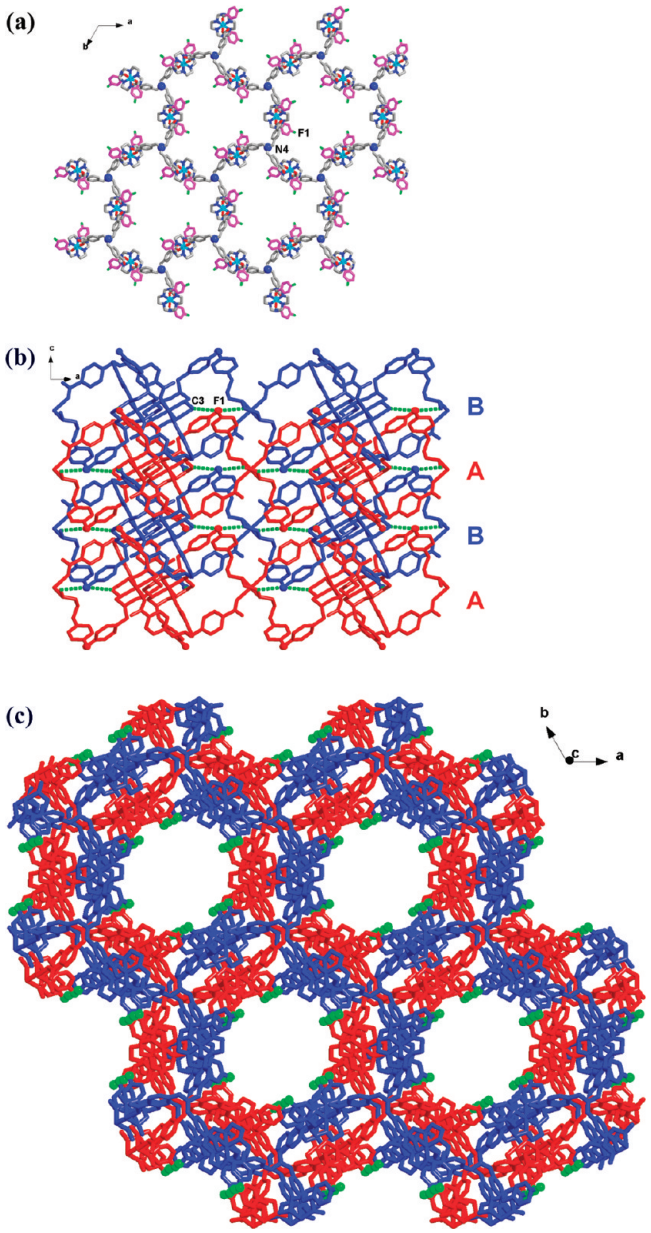

Figure 4. (a) (6,3) sheet of **3**, showing cloverleaf-shaped cavities and the tropism of 4-fluorobenzyl groups (in pink). (b) The ABAB stacking mode in **3**, showing the C−H···F hydrogen bonding interactions between adjacent sheets (A···B). (c) The 3D porous structure of **3** with 1D fluorine atoms (green) interspersed channels (the solvents are omitted for clarity).

guest molecules (6 DMF and 18 water molecules) in the temperature range 25−160 °C; the weight loss found of 24.8% is consistent with that calculated (25.2%). The desolvated framework is stable up to 220 °C, and is followed by another two steps of weight losses after that temperature. The TG curve of **3** shows an initial weight loss of 24.9% from room temperature to 160 °C, which is in good agreement with the losses of eight DMF and nine water molecules (calcd 24.8%). The desolvated framework is stable up to 225 °C, and then begins to decompose with another two steps of weight losses.

Sorption Properties. To examine the permanent porosities and storage capability, the gas adsorption properties of desolvated **2** (**2d**) and **3** (**3d**) were investigated (Figure 7). The results show that both **2d** and **3d** can adsorb N_2, H_2, and CO_2 molecules. For **2d**, the amounts of N_2 uptake increase abruptly at the beginning and reach a plateau of 187.7 cm^3 (STP)/g at 1.0 atm, presenting a typical type-I curve, indicating **2d** is a microporous material.[16] Fitting the BET and Langmuir equations to the N_2 adsorption isotherm gave estimated surface areas of 691 and 803 m^2/g, respectively. At 195 K, **2d** also exhibits good CO_2 adsorption behavior. Interestingly, the CO_2 adsorption isotherm shows two step sorption. From 0 to 0.1 atm, **2d** can adsorb 117 cm^3 (STP)/g of CO_2, and then it adsorbs more CO_2 and reaches a platform of 172 cm^3 (STP)/g. The stepwise behavior of CO_2 sorption observed in **2d** may be ascribed to the flexibility of its framework which is induced by the quadrupole moment of CO_2 molecule (-1.4×10^{-39} C m^2).[17] The hydrogen adsorption isotherm at 77 K reveals that **2d** can store 63.1 cm^3 (STP)/g (0.57%) of H_2, which is much

dx.doi.org/10.1021/ic202168r | Inorg. Chem. 2012, 51, 1874−1880

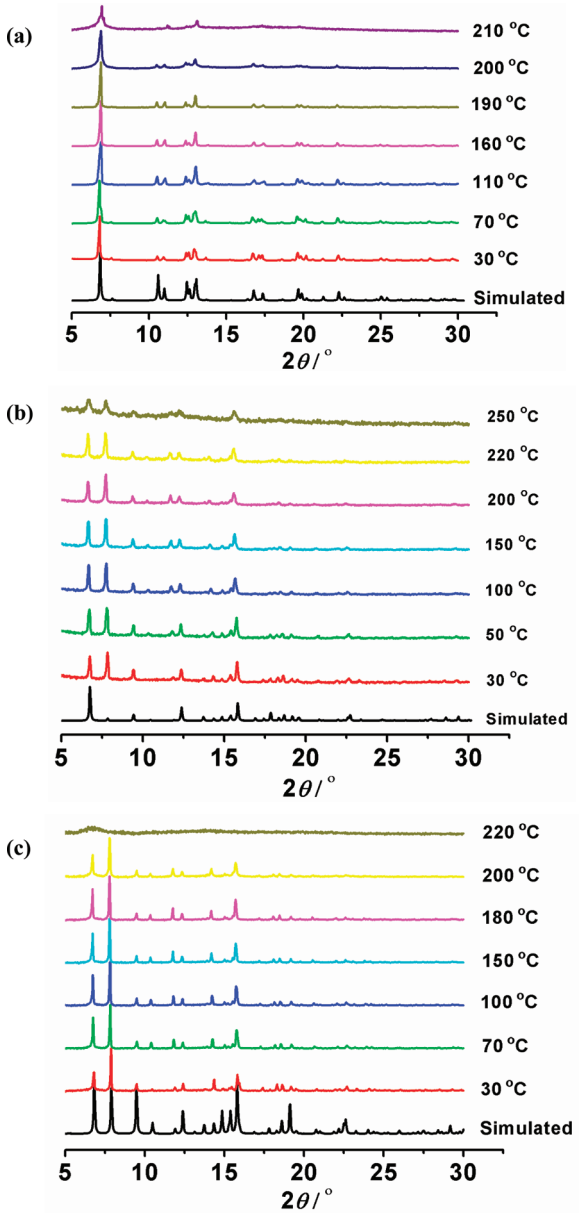

Figure 5. Variable temperature XRD patterns for (a) **1**, (b) **2**, and (c) **3**. The variable temperature XRD patterns depicted were based on as-made samples. The time for each sample staying at each temperature is 5 min.

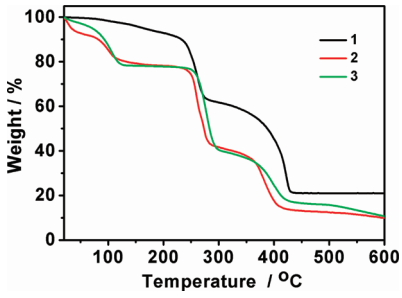

Figure 6. TG curves for **1**−**3**.

smaller than the theoretical value of 215.2 cm^3 (STP)/g (1.94%). This may be ascribed to the weak interactions between the pores and H_2 molecules.[18] The sorption behaviors of **3d** are similar to those of **2d**, and **3d** can adsorb 213.5, 74.9, and 188.4 cm^3 (STP)/g of N_2, H_2, and CO_2, respectively. These values are slightly larger than those observed in **2d** (187.7, 63.1, and 172.1 cm^3 (STP)/g).

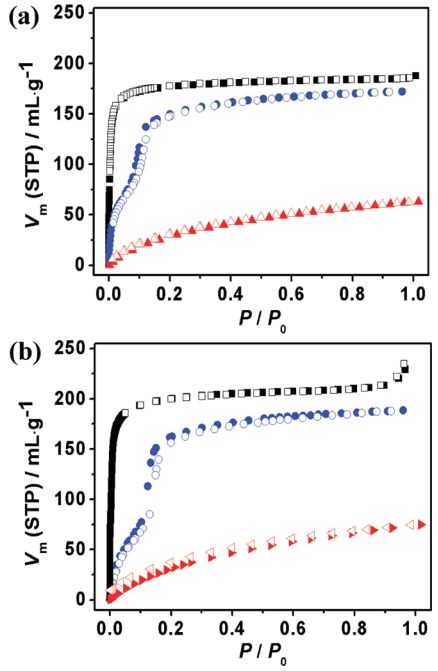

Figure 7. Gas sorption isotherms for desolvated (a) **2** and (b) **3** (black ■/□, N_2 adsorption/desorption at 77 K; blue ■/□, CO_2 adsorption/desorption at 195 K; red ■/□, H_2 adsorption/desorption at 77 K).

Recently, Cheetham and co-workers reported a partially fluorinated PCPs of $[Zn_5(triazole)_6(tetrafluoroterephthalate)_2(H_2O)_2]\cdot 4H_2O$, which displays strong binding to H_2 molecules. They reasoned that both the fluorine atoms exposed to the pore surfaces and the small pore sizes (3.7 × 6.7 $Å^2$) contributed to this strong interactions.[4d] Combined with the result of our work, we conclude that the strong binding to H_2 molecules is mainly related to the small pore sizes rather than the fluorine atom interspersed pore surface.

■ CONCLUSION

Under the same reaction conditions, altering the positions of fluorine atoms in the azamacrocyclic ligands lead to the formation of three coordination polymers with different structures and properties. **1** shows a 2D Borromean layer structure, while **2** and **3** exhibit 3D porous structures with 1D F-atoms interspersed nanosize channels. The results of gas sorption measurements indicate both desolvated **2** and **3** can adsorb N_2, H_2, and CO_2 molecules. Although the pore surfaces of desolvated **2** and **3** are functionalized with fluorine atoms, they can not strongly bind to H_2 molecules, illustrating that the small pore sizes rather than the fluorine atoms exposed to the pore surfaces contribute to the strong H_2 binding of PCPs.

■ ASSOCIATED CONTENT

Supporting Information

Selected bond distances and angles for **1**−**3**. CIF data. This material is available free of charge via the Internet at http://pubs.acs.org.

dx.doi.org/10.1021/ic202168r | Inorg. Chem. 2012, 51, 1874−1880

AUTHOR INFORMATION

Corresponding Author

*E-mail: zhong_dichang@yahoo.com.cn (D.-C.Z.); lutongbu@mail.sysu.edu.cn (T.-B.L.). Fax: +86-20-84112921.

ACKNOWLEDGMENTS

This work was supported by NSFC (20831005, 20821001, 21001119, 91127002) and 973 Program of China (2007CB815305 and 2012CB821705).

REFERENCES

(1) (a) Furukawa, H.; Ko, N.; Go, Y. B.; Aratani, N.; Choi, S. B.; Choi, E.; Yazaydin, A. Ö.; Snurr, R. Q.; O'Keeffe, M.; Kim, J.; Yaghi, O. M. *Science* **2010**, *329*, 424. (b) Mulfort, K. L.; Farha, O. K.; Malliakas, C. D.; Kanatzidis, M. G.; Hupp, J. T. *Chem.—Eur. J.* **2010**, *16*, 276. (c) Tanaka, D.; Henke, A.; Albrecht, K.; Moeller, M.; Nakagawa, K.; Kitagawa, S.; Groll, J. *Nat. Chem* **2010**, *2*, 410. (d) Bourrelly, S.; Moulin, B.; Rivera, A.; Maurin, G.; Devautour-Vinot, S.; Serre, C.; Devic, T.; Horcajada, P.; Vimont, A.; Clet, G.; Daturi, M.; Lavalley, J.-C.; Loeran-Serna, S.; Denoyel, R.; Llewellyn, P. L.; Férey, G. *J. Am. Chem. Soc.* **2010**, *132*, 9488. (e) Nouar, F.; Eckert, J.; Eubank, J. F.; Forster, P.; Eddaoudi, M. *J. Am. Chem. Soc.* **2009**, *131*, 2864.

(2) (a) Zhao, Y. G.; Wu, H. H.; Emge, T. J.; Gong, Q. H.; Nijem, N.; Chabal, Y. J.; Kong, L. Z.; Langreth, D. C.; Liu, H.; Zeng, H. P.; Li, J. *Chem.—Eur. J.* **2011**, *17*, 5101. (b) Devic, T.; Horcajada, P.; Serre, C.; Salles, F.; Maurin, G.; Moulin, B.; Heurtaux, D.; Clet, G.; Vimont, A.; Grenèche, J. M.; Le Ouay, B.; Moreau, F.; Magnier, E.; Filinchuk, Y.; Marrot, J.; Lavalley, J. C.; Daturi, M.; Férey, G. *J. Am. Chem. Soc.* **2010**, *132*, 1127. (c) Demessence, A.; D'Alessandro, D. M.; Foo, M. L.; Long, J. R. *J. Am. Chem. Soc.* **2009**, *131*, 8784. (d) Zhong, D. C.; Lin, J. B.; Lu, W. G.; Jiang, L.; Lu, T. B. *Inorg. Chem.* **2009**, *48*, 8656. (e) Deng, H. X.; Doonan, C. J.; Furukawa, H.; Ferreira, R. B.; Towne, J.; Knobler, C. B.; Wang, B.; Yaghi, O. M. *Science* **2008**, *327*, 846. (f) Li, J. R.; Tao, Y.; Yu, Q.; Bu, X. H.; Sakamoto, H.; Kitagawa, S. *Chem.—Eur. J.* **2008**, *14*, 2771. (g) Matsuda, R.; Kitaura, R.; Kitagawa, S.; Kubota, Y.; Belosludov, R. V.; Kobayashi, T. C.; Sakamoto, H.; Chiba, T.; Takata, M.; Kawazoe, Y.; Mita, Y. *Nature* **2005**, *436*, 238.

(3) (a) Chen, J.; Li, C. P.; Du, M. *CrystEngComm* **2011**, *13*, 1885. (b) Uemura, K.; Yamasaki, Y.; Onishi, F.; Kita, H.; Ebihara, M. *Inorg. Chem.* **2010**, *49*, 10133. (c) Zhou, D. S.; Wang, F. K.; Yang, S. Y.; Xie, Z. X.; Huang, R. B. *CrystEngComm* **2009**, *11*, 2548. (d) Huang, X. C.; Zhang, J. P.; Chen, X. M. *J. Am. Chem. Soc.* **2004**, *126*, 13218.

(4) (a) Pachfule, P.; Das, R.; Poddar, P.; Banerjee, R. *Cryst. Growth Des.* **2011**, *11*, 1215. (b) Lin, X.; Telepeni, I.; Blake, A. J.; Dailly, A.; Brown, C. M.; Simmons, J. M.; Zoppi, M.; Walker, G. S.; Thomas, K. M.; Mays, T. J.; Hubberstey, P.; Champness, N. R.; Schröder, M. J. *Am. Chem. Soc.* **2009**, *131*, 2159. (c) Uemura, K.; Maeda, A.; Maji, T. K.; Kanoo, P.; Kita, H. *Eur. J. Inorg. Chem.* **2009**, 2329. (d) Hulvey, Z.; Falcao, E. H. L.; Eckert, J.; Cheetham, A. K. *J. Mater. Chem.* **2009**, *19*, 4307. (e) Yang, C.; Wang, X. P.; Omary, M. A. *J. Am. Chem. Soc.* **2007**, *129*, 15454. (f) Gao, Y.; Twamley, B.; Shreeve, J. M. *Inorg. Chem.* **2006**, *45*, 1150.

(5) (a) Park, H. J.; Suh, M. P. *Chem. Commun.* **2010**, 610. (b) Choi, H. S.; Suh, M. P. *Angew. Chem., Int. Ed.* **2009**, *48*, 6865. (c) Suh, M. P.; Cheon, Y. E.; Lee, E. Y. *Coord. Chem. Rev.* **2008**, *252*, 1007. (d) Cheon, Y. E.; Suh, M. P. *Chem.—Eur. J.* **2008**, *14*, 3961. (e) Suh, M. P.; Moon, H. R.; Lee, E. Y.; Jang, S. Y. *J. Am. Chem. Soc.* **2006**, *128*, 4710. (f) Moon, H. R.; Kim, J. H.; Suh, M. P. *Angew. Chem., Int. Ed.* **2005**, *44*, 1261. (g) Choi, H. J.; Suh, M. P. *J. Am. Chem. Soc.* **2004**, *126*, 15844. (h) Lu, T. B.; Xiang, H.; Luck, R. L.; Jiang, L.; Mao, Z. W.; Ji, L. N. *New J. Chem.* **2002**, *26*, 969. (i) Lu, T. B.; Xiang, H.; Su, C. Y.; Cheng, P.; Mao, Z. W.; Ji, L. N. *New. J. Chem.* **2001**, *25*, 216.

(6) Meng, X. R.; Zhong, D. C.; Jiang, L.; Li, H. Y.; Lu, T. B. *Cryst. Growth Des.* **2011**, *11*, 2020.

(7) *CrysAlis R. E. D., Version 1.171.31.7*; Oxford Diffraction Ltd., 2006.

(8) van der Sluis, P.; Spek, A. L. *Acta Crystallogr.* **1990**, *A46*, 194.

(9) Sheldrick, G. M. *SHELXS 97, Program for Crystal Structure Refinement*; University of Göttingen: Göttingen, Germany, 1997.

(10) Cantrill, S. J.; Chichak, K. S.; Peters, A. J.; Stoddart, J. F. *Acc. Chem. Res.* **2005**, *38*, 1.

(11) Amabilino, D. B.; Pérez-García, L. *Chem. Soc. Rev.* **2009**, *38*, 1562.

(12) (a) Men, Y. B.; Sun, J. L.; Huang, Z. T.; Zheng, Q. Y. *Chem. Commun.* **2010**, *46*, 6299. (b) Meyer, C. D.; Forgan, R. S.; Chichak, K. S.; Peters, A. J.; Tangchaivang, N.; Cave, G. W. V.; Khan, S. I.; Cantrill, S. J.; Stoddart, J. F. *Chem.—Eur. J.* **2010**, *16*, 12570. (c) Byrne, P.; Lloyd, G. O.; Clarke, N.; Steed, J. W. *Angew. Chem., Int. Ed.* **2008**, *47*, 5761. (d) Zhang, X. L.; Guo, C. P.; Yang, Q. Y.; Wang, W.; Liu, W. S.; Kang, B. S.; Su, C. Y. *Chem. Commun.* **2007**, 4242. (e) Zhang, X. L.; Guo, C. P.; Yang, Q. Y.; Lu, T. B.; Tong, Y. X.; Su, C. Y. *Chem. Mater.* **2007**, *19*, 4630.

(13) Suh, M. P.; Choi, H. J.; So, S. M.; Kim, B. M. *Inorg. Chem.* **2003**, *42*, 676.

(14) Bayón, R.; Coco, S.; Espinet, P. *Chem.—Eur. J.* **2005**, *11*, 1079.

(15) Spek, A. L. *PLATON, A Multipurpose Crystallographic Tool*; Utrecht University: Utrecht, The Netherlands, 2003.

(16) Rouquerol, F.; Rouquerol, J.; Sing, K. *Adsorption by Powders and Porous Solids*; Academic Press: London, 1999.

(17) Férey, G.; Mellot−Draznieks, C.; Serre, C.; Millange, F. *Acc. Chem. Res.* **2005**, *38*, 217.

(18) Wang, X. S.; Ma, S. Q.; Forster, P. M.; Yuan, D. Q.; Eckert, J.; Lpez, J. J.; Murphy, B. J.; Parise, J. B.; Zhou, H. C. *Angew. Chem., Int. Ed.* **2008**, *47*, 7263.